Measuring the Point Spread Function of a Light Microscope

by

Anthony D. Patire

Submitted to the Department of Electrical Engineering and Computer Science

in partial fulfillment of the requirements for the degree of

Master of Engineering in Electrical Engineering and Computer Science

at the

MASSACHUSETTS INSTITUTE OF TECHNOLOGY

February 1997

Signature of Author.....

Department of Electrical Engineering and Computer Science

February 7, 1997

Certified by.....

Dennis M. Freeman

Assistant Professor of Electrical Engineering

Thesis Supervisor

Accepted by.....

Frederic R. Morgenthaler

Chairman, Department Committee on Graduate Theses

Measuring the Point Spread Function of a Light Microscope

by

Anthony D. Patire

Submitted to the

Department of Electrical Engineering and Computer Science

February 7, 1997

In Partial Fulfillment of the

Requirements for the Degree of

Master of Engineering in Electrical Engineering and Computer Science

ABSTRACT

Methods are described to measure the impulse response, or point spread function (PSF), of a light microscope. The new methods compare favorably to those used by others, which are shown to be flawed. The new methods measure a three-dimensional point target in both fluorescence and brightfield microscopy using Köhler illumination. The results closely match theoretical predictions. Simple theory does not capture all of the behavior of the microscope. A qualitative extension to the theory is given to explain discrepancies between measurements and theoretical predictions that occur in some operating regimes of the microscope.

Thesis Supervisor: Dennis Freeman

Title: Assistant Professor of Electrical Engineering

Acknowledgments

First, I would like to thank Denny Freeman for advising me throughout this thesis. His friendly encouragement was always appreciated and his enthusiasm was often contagious. I would also like to thank Zoher, Rosanne, Quentin, Laura, Cameron, and A.J. for their insight, laughter, sarcasm, patience, cynicism, and beer. It was a pleasure to work with a group of people who are even more disturbed than I am. Special thanks to Denny, A.J., Laura, and Rosanne for proofreading my thesis and offering countless suggestions and improvements. Thanks for the really great emu!

I would like to thank all my friends, past and present—you know who you are. Thank you Allen and Carrie for standing by me under the wrath of a malevolent taxi cab driver. I owe a great deal to my family without whom none of this would have been possible. Thank you mom, dad, grandmom, and grandpop for sending me to M.I.T., and thank you Mary, for being the best sister a brother could possibly have.

I rolled the dice, and I won. Thank you, God.

Contents

Chapter 1

Introduction

A light microscope is a system that maps a target to an image. For example, a two-dimensional target in the microscope plane of focus maps to a two-dimensional image. Similarly, a three-dimensional target can be considered to map to a three-dimensional volume image that is constructed from a stack of two-dimensional images, each taken with the plane of focus of the microscope slicing through a different plane of the target.

To a first order, the mapping from target to image can be modeled as a linear process [5]. The properties of a linear system are conveniently summarized by an impulse response. The impulse response of a microscope is a function of three spatial dimensions, and is generally called a point spread function (PSF). The PSF of a microscope concisely summarizes its mapping from a three-dimensional target to a three-dimensional image.

If the PSF of a microscope were known, then linear system theory could be applied to enhance images from a microscope. However, the PSF is strongly influenced by precisely how the microscope is used, and often the measured PSF does not match theoretical predictions [4]. The aims of this thesis are 1) to characterize a state-of-the-art Zeiss Axioplan microscope, 2) to compare results to theories, and 3) to describe a simple and accurate method for measuring the PSF.

For quantitative analysis, it is necessary to couple the microscope with a recording instrument. For this purpose, our system includes a CCD camera and video digitizer (Photometrics) installed on a personal computer.

Chapter two provides a basic background on optical microscopy. Köhler Illumination and Fourier Optics are introduced as well as a basic microscope model from which the theoretical PSF can be derived. Chapter three describes the important considerations and the different processes for measuring the PSF. Both the procedures for constructing a suitable test target, and the evaluation of raw data is explained. Chapter four illustrates the various measurements of the PSF in both brightfield and fluorescence microscopy. The features of these PSFs are compared to the theoretical model. Chapter five discusses the significance of these findings, and evaluates the consistency of the results.

Chapter 2

Background on Optical Microscopy

2.1 Köhler Illumination and Fourier Optics

The structure of the optics in Köhler illumination is devised such that there are two series of conjugate planes [2]. The first set of conjugate planes is marked with a single asterisk in Figure 2-1. The conjugate planes in this series are equivalent, so that objects in one plane will be sharply in focus in all other conjugate planes in the series. The field iris controls the region of the specimen plane that is illuminated by the light source. An image of the specimen appears in the primary image plane as well as on the surface of the CCD camera.

As shown in Figure 2-2, an expanding spherical wave at the focal point of a lens will be transformed into a wave that will focus at infinity. In other words, a lens will convert a spherical wave into a plane wave. The distribution of light incident upon a lens and the distribution of light on its corresponding focal plane are related by the two-dimensional Fourier Transform. This relationship is a general property of lenses [5].

The intensity distribution on the left focal plane in Figure 2-2 is a two-dimensional impulse, $\delta(x)\delta(y)$. The intensity distribution immediately to the right of the lens is the set of weights for each element of the Fourier Transform of the impulse. Another way to say this is that an expanding spherical wave (point source) can be described by a sum of plane waves each of which has an identical weight in the spatial frequency

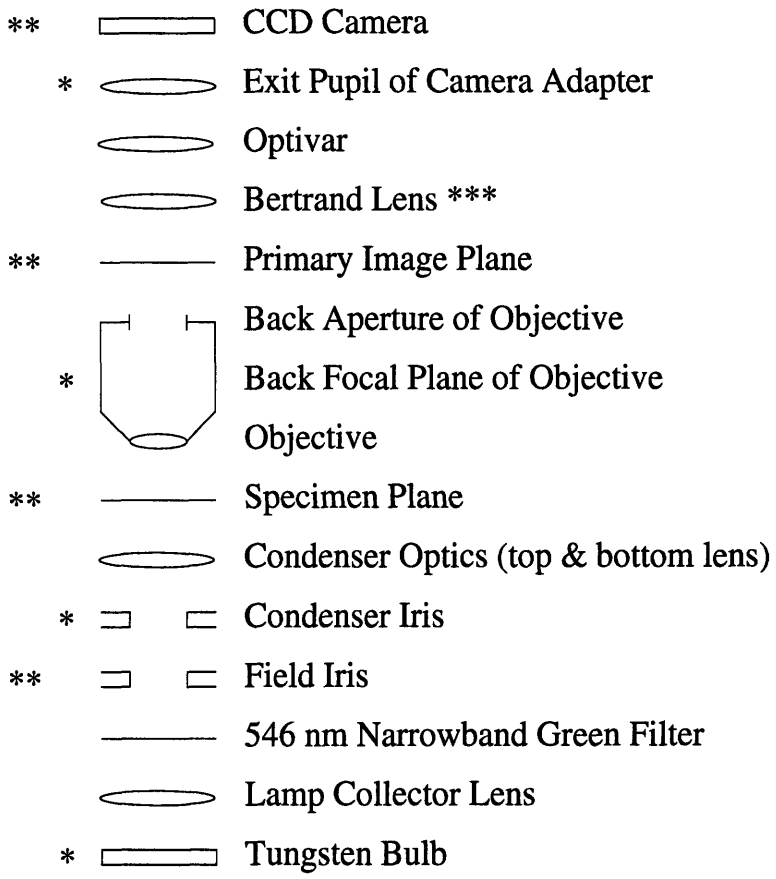

Figure 2-1: The optical path of a light microscope using brightfield illumination. The single asterisks denote the first set of conjugate planes, and the double asterisks denote the second set of conjugate planes within the optical path. The CCD camera is normally in the same conjugate set as the specimen plane as shown. The Bertrand lens is normally used to toggle the CCD Camera between the two possible sets of conjugate planes. A tungsten bulb of variable brightness is used to provide illumination. Chromatic aberrations that result because the index of refraction of glass depends on the wavelength of light are avoided by the use of a green filter (546 nm center wavelength, 30 nm bandwidth) to limit wavelengths to those for which our objective is well corrected. The objective, optivar and camera adapter provide the necessary magnification. The camera samples the output from the microscope optics.

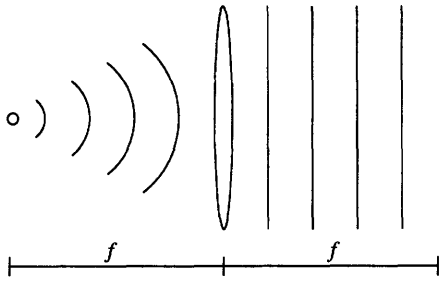

Figure 2-2: A spherical wave originating from a point source at the focal distance of a lens is converted to a plane wave.

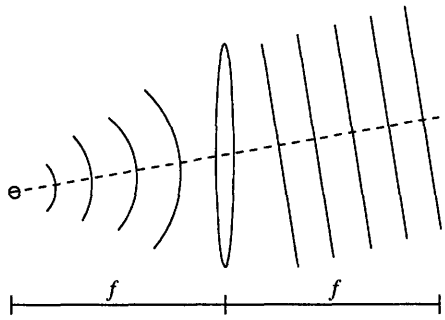

Figure 2-3: An off-axis spherical wave originating from the focal distance of a lens is converted to a plane wave travelling at an angle corresponding to the location of the point source.

domain. The Fourier Transform of an impulse is a constant.

Light can pass through a lens in either direction, indicating that a duality exists to be exploited. A plane wave normally incident on a lens will be transformed to a spherical wave converging to a single point on the focal plane. The corresponding weights for each element of the Fourier Transform that makes up this DC value is an impulse at the origin. If the point source is off-axis, then the lens will convert the resulting off-axis spherical wave into a plane wave travelling at an angle as shown in Figure 2-3 [9].

Köhler illumination exploits this Fourier Transforming property of lenses by arranging the optics so that the first conjugate plane is the Fourier Transform of the second. Consequently, each point in the tungsten bulb light source provides a plane

wave with which to illuminate the specimen from a different angle. In this way, every point of light from the tungsten bulb evenly illuminates every point in the specimen plane.

In the same way that the summation of one-dimensional cosine functions from a range of frequencies can approximate another one-dimensional waveform, the summation of plane waves from a range of the angular spectrum can approximate a two-dimensional waveform. The angular spectrum available to construct a two-dimensional waveform is analogous to the bandwidth available to construct a one-dimensional waveform.

In the specimen plane, and in the corresponding conjugate planes, a finite aperture limits the field of view. In the other set of conjugate planes (the illumination planes), a finite aperture limits the resolution of the image by limiting the angular spectrum (bandwidth) available to illuminate the specimen.

Both the objective lens and the condenser top lens have a finite aperture, or cutoff spatial frequency, which means that there is a practical limit to the range of the angular spectrum that can be focused in the final image. Therefore, the finite aperture acts as a spatial lowpass filter. The impulse response of the lowpass filter that is the objective of the microscope is called the PSF of the system.

2.2 PSF Model Based on Diffraction Limited Optics

In an ideal imaging system, an infinitesimal point in the specimen plane maps to an infinitesimal point in the image plane. Such a system would be able to resolve two points in the specimen plane separated by an arbitrarily small distance. However, in practice, this is not the case. In a real imaging system, the resolution is always limited by the diffraction effects of the finite aperture in the objective lens.

The diffraction pattern from a finite aperture has been extensively studied, and there are many approximations to Kirchhoff's expression for scalar diffraction [6]. One approximation is summarized here. A point source of light illuminates the entrance pupil with a spherical wave expanding from the origin of the specimen plane as shown

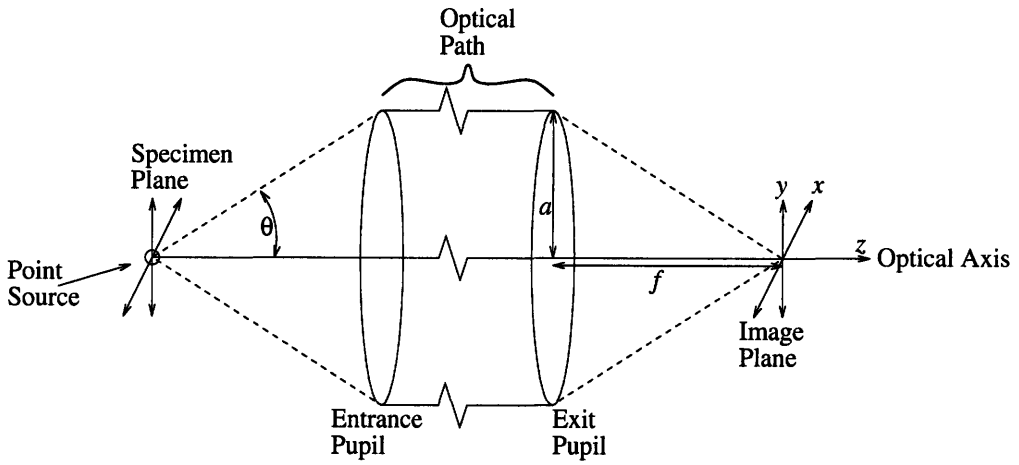

Figure 2-4: Construction to visualize the solution to the diffraction problem caused by a finite aperture of radius a. A portion of the spherical wave expanding from the point source is collected by the finite aperture of the entrance pupil. The resulting spherical wave emerging from the exit pupil converges at the origin of the image plane defined a distance f from the aperture.

in Figure 2-4. Only the light whose angle from the optical axis is less than θ will pass through the finite aperture of the entrance pupil and enter the optical path of the microscope. Light from the source at angles greater than θ will be "cut off." This phenomenon is quantified by the numerical aperture (NA) metric defined as

$$\text{NA} = n \sin(\theta) \tag{2.1}$$

where n is the index of refraction of the medium, and θ is the half angle of light incident on the aperture. In Figure 2-4 a converging spherical wave emerges from the exit pupil and focuses on the image plane. Only a fraction of the light from the point source reaches the light detector positioned on the image plane, and the result is diffraction. The three-dimensional intensity pattern $I(u, v)$ resulting from a converging spherical wave in the neighborhood of the origin of the image plane can be described by

$$I(u, v) = \left(\frac{2}{u}\right)^2 [U_1^2(u, v) + U_2^2(u, v)] I_0 \tag{2.2}$$

where I_0 is the intensity at the focus, $U_n(u, v)$ is the nth Lommel function, and u and v are normalized spatial variables [1]. The Lommel function can be written as

$$U_n(u,v) = \sum_{s=0}^{\infty} (-1)^s \left(\frac{u}{v}\right)^{n+2s} J_{n+2s}(v) \tag{2.3}$$

where J_n is the nth order Bessel Function of the first kind, and the normalized spatial variables are defined by

$$u = \frac{2\pi}{\lambda}\left(\frac{a}{f}\right)^2 z \tag{2.4}$$

$$v = \frac{2\pi}{\lambda}\left(\frac{a}{f}\right)\sqrt{x^2+y^2} \tag{2.5}$$

where a is the radius of the aperture, f is the focal distance of the lens, and λ is the optical wavelength of the light. The distribution of intensity is cylindrically symmetric about the optical axis, and easy to visualize if only one axis is considered at a time. Setting $u = 0$ in Equation 2.2 simplifies the expression into the familiar Airy formula,

$$I(0,v) = \left(\frac{2J_1(v)}{v}\right)^2 I_0 \tag{2.6}$$

which describes the intensity of light in the geometrical focal plane (the image plane orthogonal to the optical axis). Notice that it is circularly symmetric about the origin. Setting $v = 0$ in Equation 2.2 simplifies the expression to

$$I(u,0) = \left(\frac{\sin(u/4)}{u/4}\right)^2 I_0 \tag{2.7}$$

which describes the intensity distribution along the optical axis (orthogonal to the image plane).

Figure 2-5 illustrates the intensity pattern along the x and z axes. The plot is scaled for the parameters of our Zeiss 40x water immersion objective with a 1.95 mm working distance and NA of 0.75 used in this study. The information about the focal length f was provided from the manufacturer [8], however, the radius of aperture a was not.

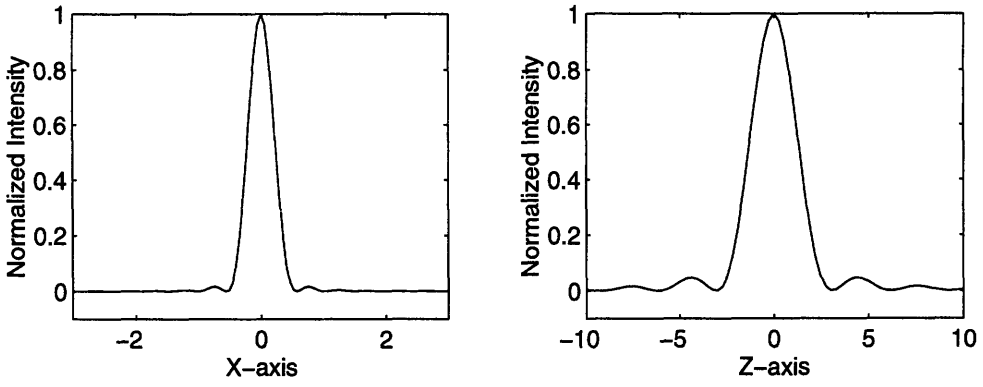

Figure 2-5: Plots of the intensity distribution of light in the region of focus from a converging spherical wave at a circular aperture. The parameters used for this calculation include radius of aperture a of 2.45 mm, focal length f of 4.11 mm, and wavelength of light λ of 546 nm. Both the x and z axes are scaled in μm.

2.3 Experimental Determination of Model Parameter

To compare measured data with the theoretical model, it was necessary to measure the radius of aperture a of the Zeiss 40x objective used in this study.

The first step was to setup the microscope in Köhler illumination. The Bertrand lens focused the image of the condenser iris onto the CCD camera. The condenser iris was opened to completely fill the back focal plane of the objective. Finally, the image of the back focal plane was captured and saved to disk. The second step was to adjust the Bertrand lens to focus on the back aperture of the objective, and to acquire an image of the back aperture.

The diameter of the back aperture of the objective was measured to be 6.48 mm in diameter. The image of the back aperture was measured to have a diameter of 500 pixels. The image of the illuminated area in the back focal plane had a diameter of 378 pixels. The comparison of the relative sizes of the image of the back aperture with the image of the back focal plane, yielded an estimate for the aperture radius of the objective a of 2.45 mm.

Chapter 3

Methods

3.1 Measuring the PSF

3.1.1 Experimental Setup: Overview

The imaging system described in this chapter consists of a Zeiss Axioplan light microscope using a Zeiss 40x water immersion objective with a 1.95 mm working distance and numerical aperture (NA) of 0.75. This system is fitted with a CCD camera and a video digitizer card (Photometrics) installed on a personal computer. The images are sampled by the camera and stored to disk. The specimen stage is connected to a stepper motor, and its position is automatically controlled by the computer. The system is capable of automatically taking a volume measurement of a target by recording images over a range of planes of focus within the specimen.

3.1.2 Sampling the Image

Whenever one uses a CCD camera or any other sampling device, care must be taken that the samples occur at a rate to avoid aliasing, and to insure that the sampled signal is a good representation of the actual signal. To do this, we need to investigate the spatial frequencies that need to be sampled by our CCD.

The resolution of a microscope is limited by the NA of the objective and the wavelength of light used to generate the image. The spatial frequency at which the

contrast in the microscope image approaches zero is called the cutoff frequency. For our system, the cutoff spatial frequency is $f_c = \frac{2NA}{\lambda} = 2.77\mu\text{m}^{-1}$ [9].

The field of view of the CCD camera is 382x576 pixels. Each pixel is 23 μm square. To avoid aliasing, the image plane must be sampled at a spatial frequency greater than twice the cutoff frequency. At a magnification of 400x, each pixel in the image plane corresponds to a square of length $l = 0.0575$ μm in the specimen plane. This rate corresponds to a sampling frequency of $f_s = 17.4$ μm^{-1} which is well above the Nyquist criteria. At this rate, aliasing is not a problem.

Not only is it important to avoid aliasing within the plane of each two dimensional image (in the x and y directions), but since we are dealing with three-dimensional volumes of data, it is also important to sample at an appropriate rate in the z direction. The depth of focus for our system is given by:

$$\Delta z = \frac{\lambda}{4n(1 - \sqrt{1 - (\frac{NA}{n})^2}}$$

where the wavelength of light, λ is 546 nm, the numerical aperture of the objective, NA is 0.75, and index of refraction of water, n is 1.333 [10]. The depth of focus is about 0.6 μm. We sampled at increments of 0.27 μm in the z direction.

3.1.3 Two-Dimensional Step Target

To measure the PSF, it is necessary to choose an appropriate target or input with which to characterize the system. The first major approach is to measure a step response by blocking half of the field of view in brightfield illumination. The derivative of the step response yields the line spread function (LSF) . Others have asserted that the LSF is equivalent to the PSF if the PSF of the lens is circularly symmetric [10]. However, the LSF is actually composed of a series of overlapping PSFs arranged in a straight line. Therefore, the LSF is at best only an approximation to the PSF.

Initial experiments involving the measurement of the step response involved the imaging of an optical slit (Ealing #43-5982) placed in the specimen plane of the microscope. At high magnification, imperfections in the slit were readily apparent.

The slit failed to provide a clean straight edge. Later experiments used a common razor blade in place of an optical slit. The razor blade had two major advantages over the optical slit for this application. The first advantage is that its cost is several orders of magnitude less than that of the optical slit. The second advantage is that the razor blade has a much cleaner and more straight edge from which to obtain a quality image.

3.1.4 Three-Dimensional Point Target

The second major approach to measuring the PSF is to build a target consisting of small microspheres dispersed in a gel or other mounting medium. This approach leads to a direct measurement of the PSF. Unfortunately, microspheres are not trivial to use. They must be small with respect to the resolution of the microscope in order to simulate an impulse in space. Therefore, by their nature, they are difficult to visualize in the microscope. Both 0.2 μm and 0.5 μm diameter microspheres manufactured by Polysciences Inc. were chosen to approximate an impulse. When performing an experiment, it is vital that one can differentiate a microsphere from a piece of dust or grime corrupting the optical path. The solution to this problem is to use fluorescent microspheres. The target can then be viewed in fluorescence microscopy to find a microsphere and to be certain that one was actually viewing a microsphere, assuming that typical dust and grime do not fluoresce. After focusing on a microsphere in fluorescence microscopy, one can measure the fluorescence PSF. One can also switch to brightfield microscopy while keeping the same bead in focus to measure the brightfield PSF.

Microspheres in Gel

The 40x objective used in this project is not corrected for use with a coverslip. Therefore, in order to accurately measure the PSF, it is necessary to build targets that do not have a coverslip. At the same time, the microspheres need to be held in a fixed position while they are being imaged. Therefore, a dispersion of microspheres is

immobilized in a gel.

In initial experiments the targets thus constructed did not work effectively. The use of a water immersion lens requires a water droplet to be situated immediately between the objective and the target. This arrangement is very useful for most applications involving biological samples. Unfortunately, due to a difference in osmotic pressure between the water droplet and the gel, solvent transport occurs, and the gel swells causing significant motion of the microsphere. Therefore, the gel initially failed to hold the microsphere in a fixed location.

To alleviate this dilemma, the osmolarity of the solutions involved in constructing the targets is controlled more carefully. Instead of making the gel as a mixture of water and gelatin, the gel is made as a mix of modified artificial endolymph (MAE) solution and gelatin. The rationale for the choice of MAE is that MAE is a commonly used solution in our laboratory, and its presence increases the osmolarity and controls the pH of the gel. Instead of using a water droplet between the objective and the gel, a droplet of MAE is used instead. Therefore, both the osmolarity of the gel and the droplet are determined by the MAE solution.

MAE contains (in mmol/L): NaCl (1.5), KCl (174), Hepes (5), dextrose (5), and sucrose (50). The pH of MAE is adjusted to 7.3. The recipe for the construction of gelatin targets is as follows. One gram of research grade gelatin (Sigma) is mixed into 40 mL of MAE, and heated until dissolved. To this mixture, microspheres, originally provided in a dispersion of 2.5% solids from the vendor, are added at a concentration of 5 μL per 10 mL MAE gelatin mixture. From this, 30 μL of the resulting solution is placed inside a trough created by an o-ring glued to a microscope slide. The preparation is sealed in a petri dish, and stored in a refrigerator to set overnight.

Microspheres in Mount-Quick

Several targets were constructed with a coverslip to evaluate the significance of spherical aberration caused by incorrect coverslip thickness. These targets are constructed by first diluting the microsphere concentration by mixing 10 μL of microsphere solution from the vendor with 10 mL of water. Next, 10 μL of the resulting solu-

tion is mixed with 3 drops of Mount-Quick (Electron Microscopy Sciences) mounting medium. Thirty μL of the final mixture are transferred to a slide, covered with a coverslip, and let set overnight. Lastly, the square coverslip/slide perimeter is coated with clear nail polish to strengthen and protect the target.

3.2 Data Analysis

3.2.1 Two-Point Correction

Raw images from the CCD camera are processed by two-point correction to reduce fixed pattern noise, and to improve image quality [3]. There are two types of fixed pattern noise—multiplicative and additive noise. For example, if the CCD camera takes a picture while the shutter is closed, it will not measure an even field of zero intensity across the CCD. The thermal production of hole-electron pairs will cause charge to be deposited across the CCD. The intensity of this so-called dark image (of additive noise) will depend on the exposure time used to take the picture. If a picture of empty space in the specimen plane is taken (with the shutter open), one would not observe an even intensity measurement across the CCD. Dust and other particles that contaminate the optical path can be modeled as having a multiplicative light absorbance. The intensity pattern measured at different points of observation across the image plane will be scaled differently (from the absorbing effect of dust), but fortunately this pattern is also consistent and correctable. For every set of PSF measurements, both a light background image as well as a dark image (taken with the closed shutter) is recorded. These measurements are then used to reduce the fixed pattern noise:

$$\mathsf{outpic(i,j)} = \frac{\mathsf{inpic(i,j)} - \mathsf{dark(i,j)}}{\mathsf{back(i,j)} - \mathsf{dark(i,j)}} \mathsf{average(back(i,j)} - \mathsf{dark(i,j))} \tag{3.1}$$

where outpic denotes the two-point corrected output, inpic is the raw input image, dark is the dark (additive noise) image, back is the bright (multiplicative noise) image, and i and j are indices of the data images.

3.2.2 Normalization and Statistics

It is important to consistently normalize the data so that PSF measurements in bright-field microscopy can be compared to PSF measurements in fluorescence microscopy. Additionally, data taken from the same microsphere at different times will have a slightly different DC-offset, and it is important to be able to compare these kinds of results in a systematic way. The first step is to define a shifting algorithm so that the background, or apparently empty, region of the image can be defined to have an intensity of zero. This facilitates the comparison of the change in intensity caused by the target.

From each volume measurement, the global extremum is found and a frame of reference is defined with this extremum at the origin. Note that the mapping of the extremum of each waveform to the origin does not correct for subpixel shifts in the waveform. The x, y and z axes are aligned with the original microscope axes. The intensity values along the new x and z axes are used to calculate statistics about the given volume of data. In general, the intensity values along the x axis at the edge of each image always consists of an apparently empty region. Therefore, the average of the 21 pixel values at each edge of the x axis, farthest away from the effect of the microsphere, is defined as the baseline pixel value. This baseline pixel value is subtracted from the intensity data along both x and z axes, yielding a set of data with the background intensity defined as zero.

For the purpose of statistical analysis, it is important to create a consistent means of defining the width of the PSF. From the shifted dataset, it is intuitive to define the region of the PSF where the intensity values along the x axis are within one half of its extremum to be the width of the PSF. This definition when applied to the intensity values along the z axis yields the height of the PSF.

3.3 Index of Refraction of Gel

A coverslip is a source of spherical aberration if used in conjunction with an objective that is not corrected for use with one. In Figure 3-1, the light emerging from a point

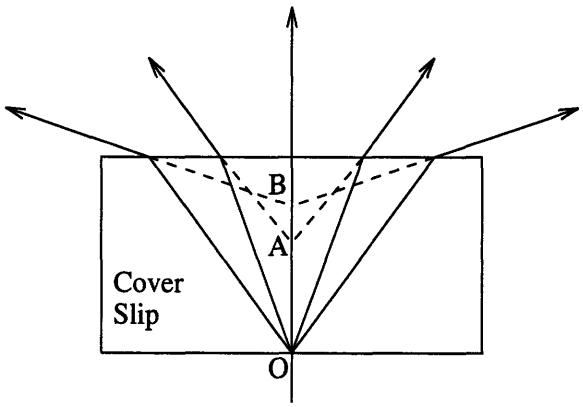

Figure 3-1: Spherical Aberration. The coverslip has an index of refraction greater than that of the surrounding medium. From above, rays of light emerging from a single point O beneath the coverslip will appear to originate from a range of points like A or B.

source underneath a coverslip (usually of crown glass n = 1.515) appears to come from a variety of sources such as points A and B [2]. The motivation for creating gel targets is to avoid this spherical aberration. Of course, gel targets will only avoid spherical aberration if the index of refraction of the gel is close to the index of water. Therefore, it is important to measure the index of refraction of the gel.

Snell's law describes the refraction of light at the boundary of two materials of differing indices of refraction. This relationship,

$$n_1 \sin(\theta_1) = n_2 \sin(\theta_2) \tag{3.2}$$

together with the geometrical construction in Figure 3-2 yields an expression,

$$n_2 = \frac{n_1 \sin(\theta_1)}{\sin(\tan^{-1}(\frac{m}{t}\tan(\theta_1)))} \tag{3.3}$$

for the index of refraction of the mounting medium n_2. The small angle approximation simplifies Equation 3.3 to,

$$n_2 = \frac{n_1 t}{m} \tag{3.4}$$

an expression that suggests a simple method to measure the index of refraction of the mounting medium. One merely needs to take two measurements: 1) the thickness of

the mounting medium, 2) the difference in the axial position of the specimen stage at which the microscope is in focus at position Q (underneath the mounting medium) and position P (outside the mounting medium) as displayed in Figure 3-3.

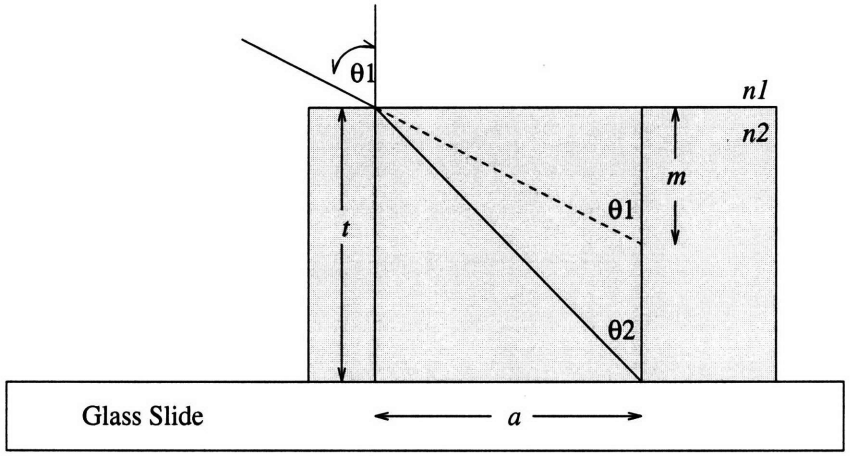

Figure 3-2: Geometrical construction to illustrate the derivation of the method to measure the index of refraction n_2 of a mounting medium. The angles θ_1 and θ_2 are the angles of incidence and refraction, respectively of a ray of light. The shaded region represents the mounting medium of thickness t with index of refraction n_2. The surrounding region above the mounting medium has an index of refraction n_1.

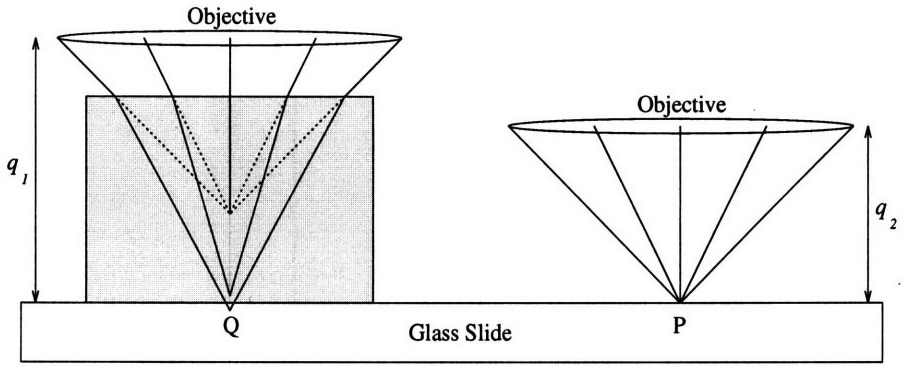

Figure 3-3: Geometrical construction to illustrate the measurement of the index of refraction n_2 of a mounting medium. Viewed through MAE, the target at point P appears to be a distance q_2 from the lens. Viewed through mounting medium, the target at point Q appears to be a distance q_1 from the lens. The difference between q_1 and q_2 is equal to the difference between t and m in Figure 3-2.

Chapter 4

Results

4.1 Repeatability of Measurements

Figure 4-1 shows a set of measurements in brightfield illumination from four different 0.5 μm microspheres. The data was taken in a successive series of experiments on the same day. The values of the waveforms, when aligned by their peaks are generally within 20% of each other. The ratio of the energy in the waveforms with the energy in their differences are compared for several different cases. For measurements taken on the same day with the same microsphere, the ratios are 18dB, and 16dB for the x and z directions respectively. For measurements taken on the same day with different microspheres, the ratios are 22dB, and 14dB for x and z directions respectively. For measurements taken on different days with different microspheres, the ratios are 19dB and 17dB respectively.

In Figure 4-1 between 4 and 10 μm above the minimum, the waveform is primarily flat. However, between 4 and 10 μm below the minimum, each waveform displays a consistent damped ringing. This ringing is visible in most PSF measurements. In Figures 4-2 and 4-3, there exists a fairly consistent checkerboard pattern beneath the dark minimum in brightfield (or bright maximum in fluorescence) in each image. The corresponding intensity plots also exhibit a ringing behavior along the negative z axis.

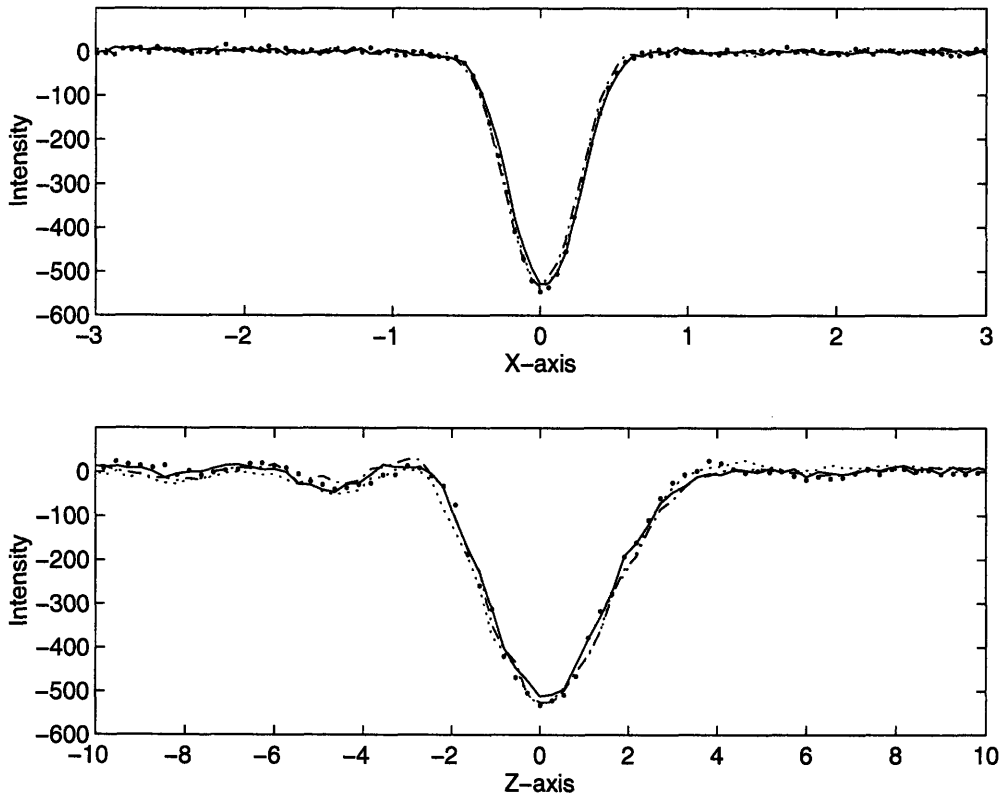

Figure 4-1: Comparison of measured data from four different microspheres in bright-field microscopy. Each set of data was taken on the same day from different 0.5 μm microspheres from the same gel-microsphere dispersion target. This set was taken with a condenser top lens with a NA of 0.9, and condenser iris NA of 0.7.

4.2 Fluorescence Microscopy

One measurement of a 0.2 μm diameter microsphere in fluorescence microscopy is displayed in Figure 4-2. For every PSF measurement, a volume of data was gathered by sweeping the plane of focus 17 μm above and below the microsphere and taking a picture at every 0.27 μm increment. In general, the measured PSF is circularly symmetric on each xy slice. The intensity values of the fluorescence measurement below the microsphere display a strong checkerboard pattern, but above the microsphere, the checkerboard pattern is almost nonexistent. The contrast between the peak intensity and the background intensity is larger in fluorescence microscopy than it is in brightfield. For the data shown in Figure 4-2, the width of the PSF along the x axis is 0.4 μm, and the height along the z axis is 3 μm.

Figure 4-2: (Next Page) Measurement of a 0.2 μm microsphere in fluorescence microscopy. The microsphere is excited with 450 to 490 nm light. The peak emission wavelength is 540 nm. The data on all of the following figures are taken with a Photometrics CCD camera mounted atop a Zeiss Axioplan microscope. The magnification of the microscope is at 400x, such that each camera pixel in the image plane corresponds to a 0.0575 μm square in the object plane. The picture on the left is the intensity pattern in the x,z plane taken through the center of the PSF, and it is displayed to scale extending 10 μm wide by 20 μm tall. Below the xz picture is a plot of the intensity values along the optical (z) axis. The images in the center stack correspond to slices of the PSF from different xy planes spaced 1.36 μm apart. To the right of each slice is a plot of the corresponding intensity values along the x-axis taken through the center of each slice.

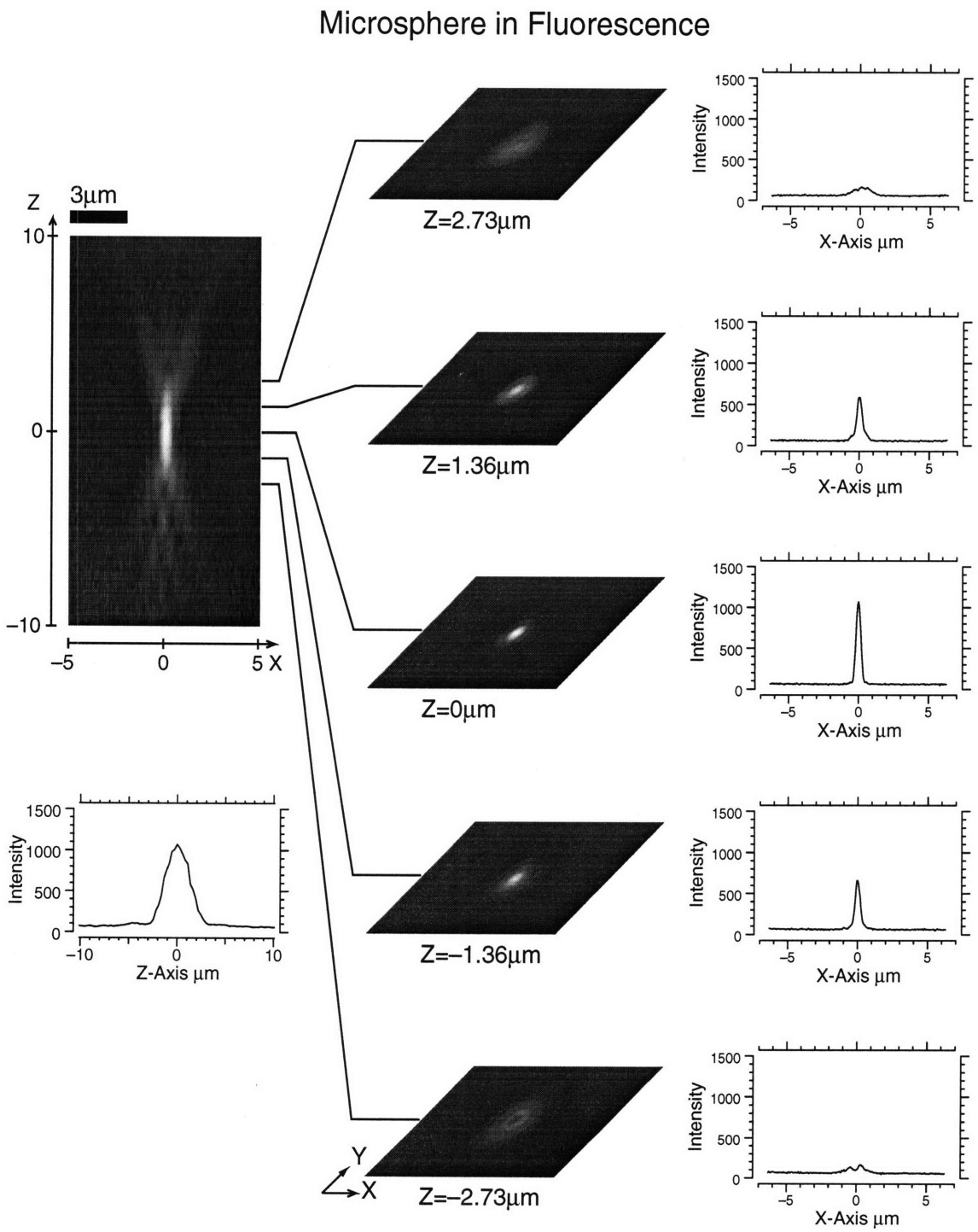
Microsphere in Fluorescence
Z
3µm
10
0
−10
−5
0
5 X
Z=2.73µm
Z=1.36µm
Z=0µm
Z=−1.36µm
Z=−2.73µm
Y
X
Intensity
1500
1000
500
0
−10
0
10
Z-Axis µm
−5
0
5
X-Axis µm

4.3 Brightfield Microscopy

4.3.1 Effect of Microsphere Size

Figure 4-3 compares results from two sets of measurements of different sized microspheres taken in brightfield microscopy. The images and the data plotted beneath each image are the two-point corrected output from the fixed pattern noise reduction algorithm described in Chapter 3. Unlike the intensity plots in Figure 4-1, all of the intensity plots in z for data in Figure 4-3 exhibit a maximum corresponding to a bright spot. Note that the data in Figure 4-1 was taken with a different condenser top lens.

The measurements of the 0.2 μm microsphere and the 0.5 μm microsphere in gel are very similar. However, the measurement from the 0.5 μm microsphere is slightly larger in size, and greater in contrast. Notice the contrast between the dark spot intensity and the background intensity for the 0.2 μm microsphere is less than half the contrast for the 0.5 μm microsphere.

4.3.2 Effect of Condenser Iris NA

Figures 4-4 and 4-5 show results from the measurement of a 0.5 μm microsphere mounted in a gel. The microsphere is illuminated in brightfield microscopy. Unlike the measurements in Figure 4-3, this set is taken with a condenser stage top lens with a NA of 0.9. The data from the 0.5 μm microsphere with the 0.6 NA top lens (Figure 4-3) is similar to the the data taken with the 0.9 NA top lens and the condenser iris set at an effective NA of 0.6 (Figure 4-4). The condenser iris is adjusted to illuminate the microsphere with an angular spectrum of light ranging in an effective NA from 0.7 to 0.2. Notice that as the NA is decreased, the measurement radically changes.

When the condenser iris NA is 0.7, which almost completely fills the NA of the objective lens, the resulting measurement very closely resembles the measurement for the 0.2 μm microsphere in fluorescence except that it is slightly larger and in reverse video. As the effective NA of the condenser iris is reduced to 0.6 as shown in Figure 4-4, the main lobe in the z direction shrinks. Bright sidelobes begin to form. As the NA

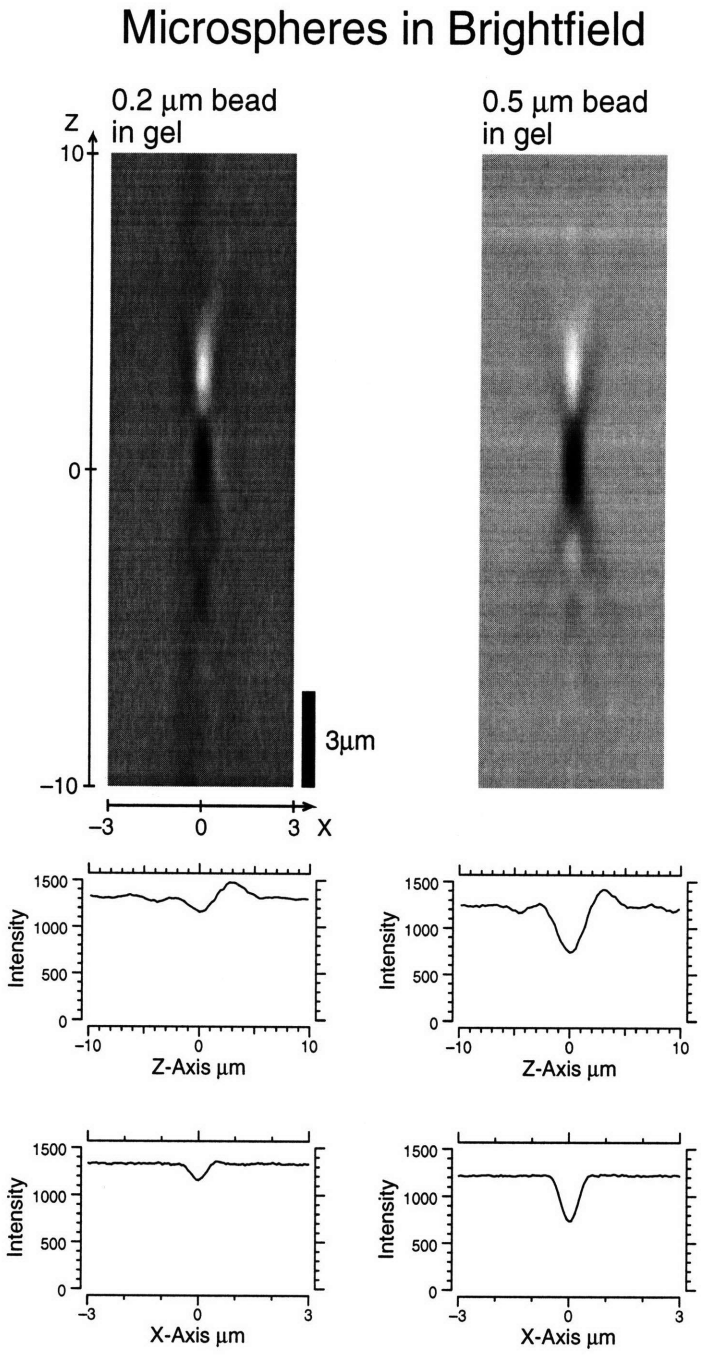

Figure 4-3: Effect of microsphere size in brightfield microscopy. Each image is to scale measuring 6 μm wide by 20 μm tall. The left column displays the results from the measurement of a 0.2 μm diameter microsphere mounted in gel with a 0.6 NA condenser top lens and an open condenser iris. The width of the PSF along the x axis is 0.46 μm. The extent of the main dark lobe in the z direction is 2.2 μm. The right column displays the results from a 0.5 μm microsphere illuminated as above. The width along the x and z axes is 0.52 μm and 2.5 μm respectively.

	Width of Dark Main Lobe in μm	
NA	x-direction	z-direction
0.7	0.58	3.3
0.6	0.52	2.5
0.5	0.52	2.5
0.4	0.52	2.5
0.3	0.52	2.5
0.2	0.58	5.2

Table 4.1: Dimensions of the dark lobes of the PSF measured under a range of condenser iris settings.

is decreased further, the main dark lobe starts to blend in more with the background, and begins to merge with the second minor lobe beneath. At an effective NA of 0.2, the minor lobe becomes indistinct from the major lobe, and their combined height in z is twice that of lobes of the other measurements. The relative sizes of the dark lobes for the condenser iris series of measurements is summarized in Table 4.1.

Figure 4-6 plots the intensity values of the measurement for a range of condenser iris settings. The intensity values are shifted so that the background intensity is identical for each measurement. Different settings of the numerical aperture of the condenser iris map to different characteristics of the bright spot. As the NA is reduced from 0.7 to 0.6, the contrast between the dark spot and the background increases. At 0.6, bright spots form both above and below the dark spot. Between 0.6 and 0.5, the relative intensity of the dark spot with respect to the background intensity remains constant. However, an intense bright spot forms primarily above the dark spot. Among all of the measurements, the one corresponding to a NA of 0.5 has the greatest contrast. Between 0.5 and 0.4, the intensity of the bright spot with respect to the background grows very slightly. However, the intensity of the dark spot with respect to the background decreases. Between 0.4 and 0.2, the contrast in the image only decreases.

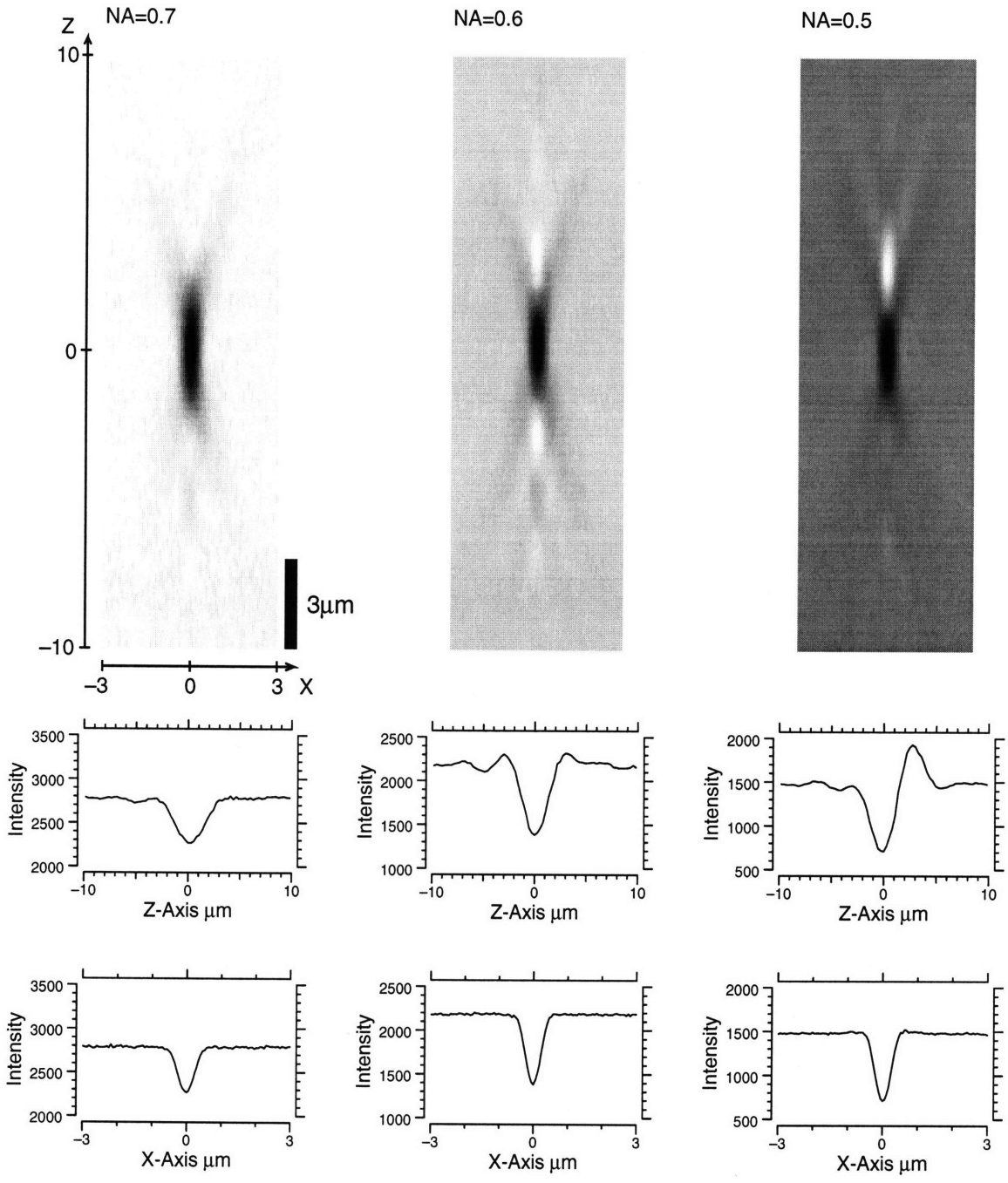

Figure 4-4: Effect of condenser iris NA on the measurement of a 0.5 μm microsphere mounted in a gel. The microsphere is illuminated in brightfield microscopy with a 0.9 NA top lens. The three columns correspond to measurements taken with the NA of the condenser iris at 0.7, 0.6 and 0.5 (from right to left).

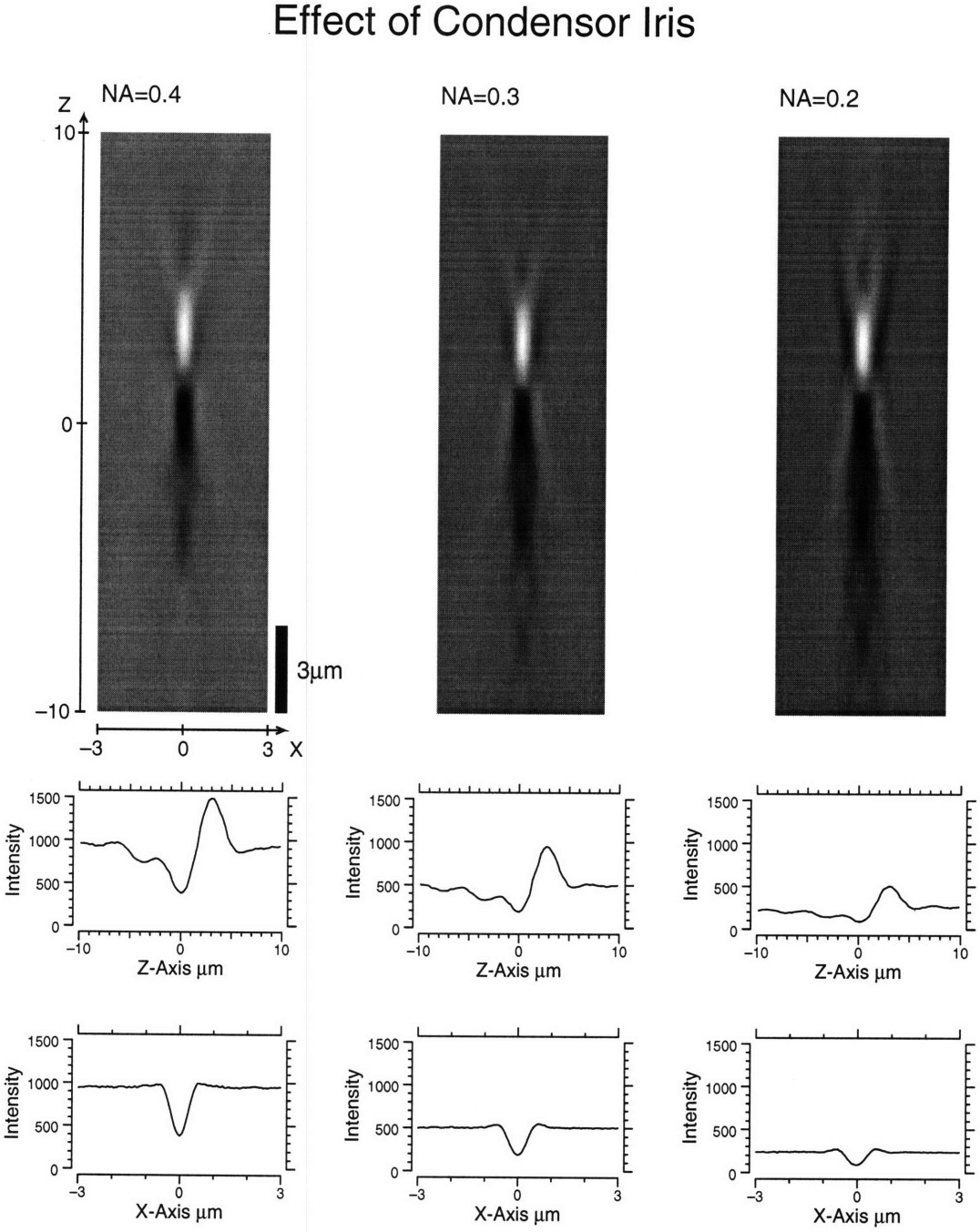

Figure 4-5: Effect of condenser iris NA on the measurement of a 0.5 μm microsphere mounted in a gel. The microsphere is illuminated in brightfield microscopy with a 0.9 NA top lens. The three columns correspond to measurements taken with the NA of the condenser iris at 0.4, 0.3 and 0.2 (from right to left).

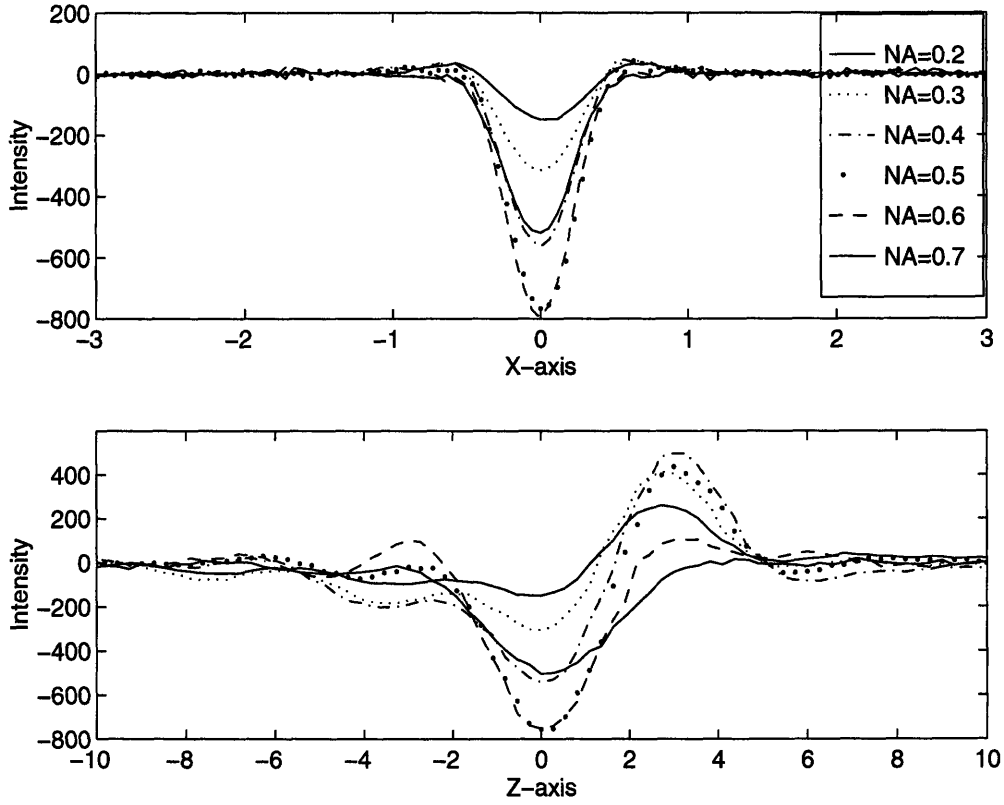

Figure 4-6: Comparison of intensity values for the measured data along the major axes for a range of condenser iris settings with an effective NA from 0.7 to 0.2. The top solid line corresponds to a NA of 0.2. The bottom solid line corresponds to a NA of 0.7.

4.4 Effect of Aberrations

4.4.1 Chromatic Aberration

A previous study that attempted to measure the PSF report results that differ from those shown here [4]. One possible explanation for this discrepancy could be the effect of chromatic or spherical aberrations.

Chromatic aberrations occur as a result of the fact that the index of refraction in glass is a function of wavelength. Figure 4-7 shows the effect of chromatic aberration on a PSF measurement in brightfield. The data for this plot have been shifted to equalize the background intensity. Notice that when no green filter is present, the waveform has about one third of the contrast and is almost twice as tall in z.

4.4.2 Spherical Aberration

The effect of a coverslip in fluorescence microscopy is shown in Figure 4-8. Data collected for a 0.2 μm diameter microsphere mounted in Mount-Quick (Electron Microscopy Sciences) with a coverslip is compared to the results for a 0.2 μm microsphere mounted in a gel, also in fluorescence microscopy. The major difference between these two measurements is that the target with the coverslip has a bump in the intensity pattern between -4 and -2 μm along the z axis.

In brightfield illumination, the effect of a coverslip is to increase the intensity of the bright spot, and to extend the dark lobe in z as shown in Figure 4-9. The shape of the main dark lobe has a camel-back hump—similar to those measurements taken at low condenser NA (Figure 4-5). The main dark lobe and the minor dark lobe beneath have both been extended in z such that they have ceased to be distinct from one another. Also, the bright spot above the microsphere has a greater contrast with respect to the background than the dark spot—again, this phenomenon is similar to those measurements taken at low condenser NA.

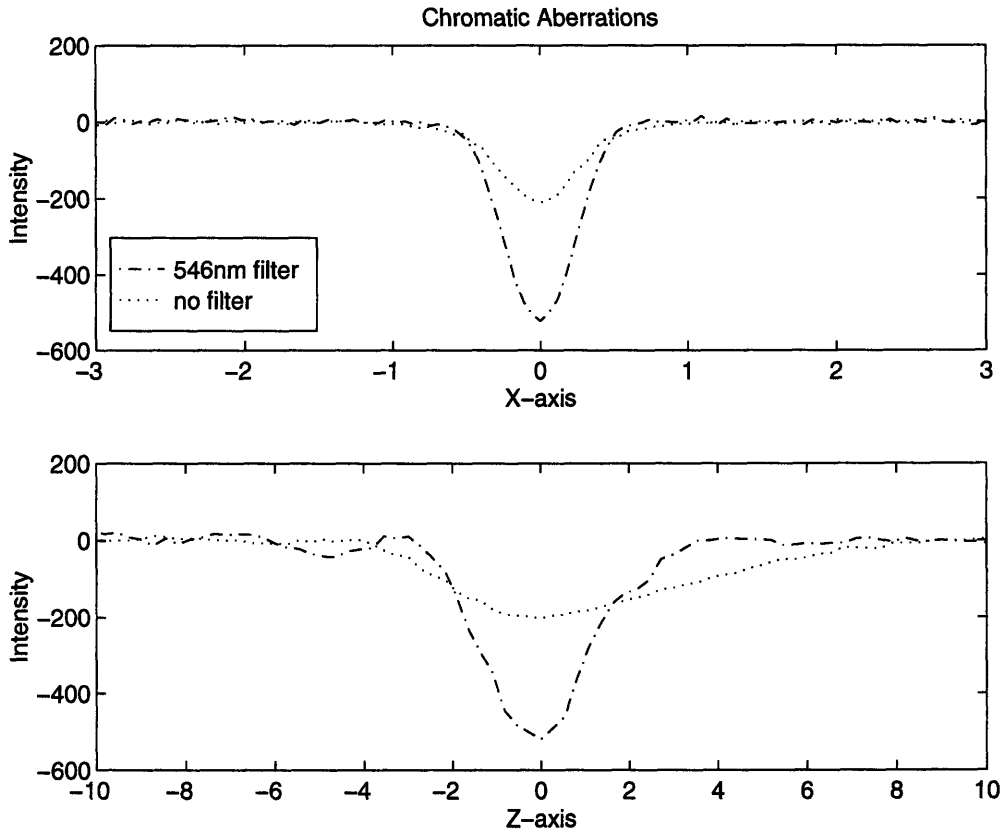

Figure 4-7: The effect of chromatic aberration on the PSF measurement. Both sets of data are taken from a 0.5 μm microsphere in gel in brightfield illumination. The dotted line shows the measurement when only a neutral density filter is present. The dashed dotted line shows the measurement when a green filter (546 nm center wavelength, 30 nm bandwidth) is present.

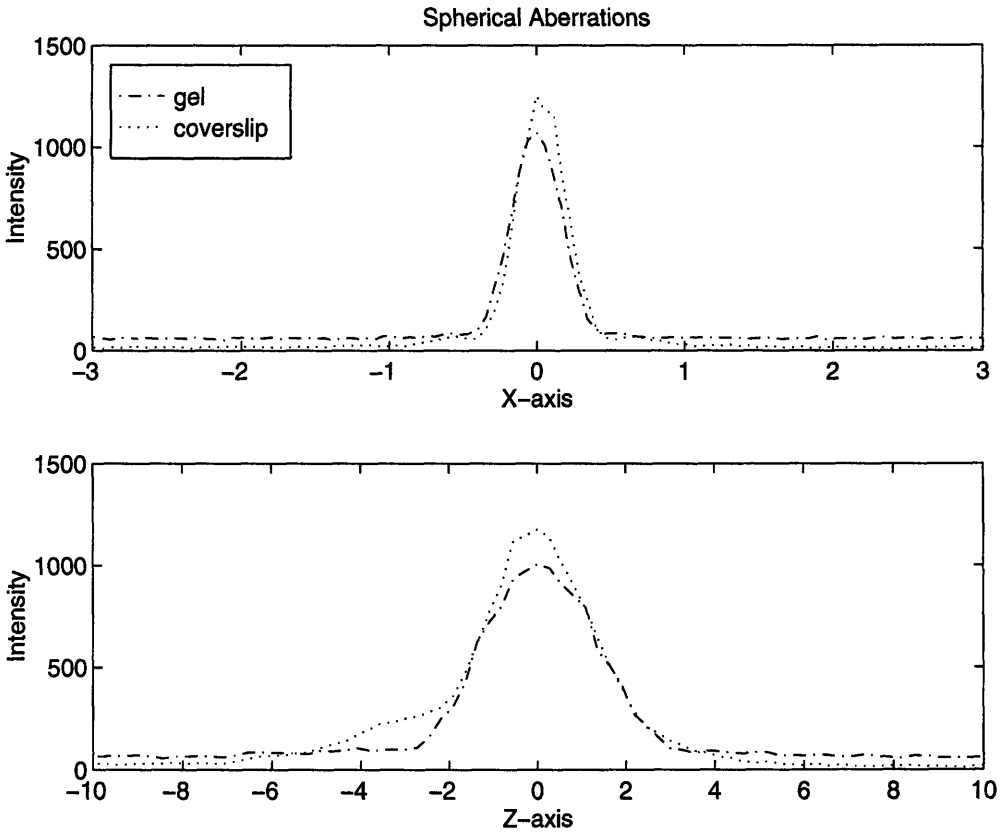

Figure 4-8: The effect of spherical aberration on the PSF measurement. Both sets of data are taken from a 0.2 μm microsphere in fluorescence microscopy. The dotted line corresponds to data taken from a microsphere mounted in Mount-Quick underneath a coverslip. The dashed dotted line corresponds to data taken from a microsphere in gel.

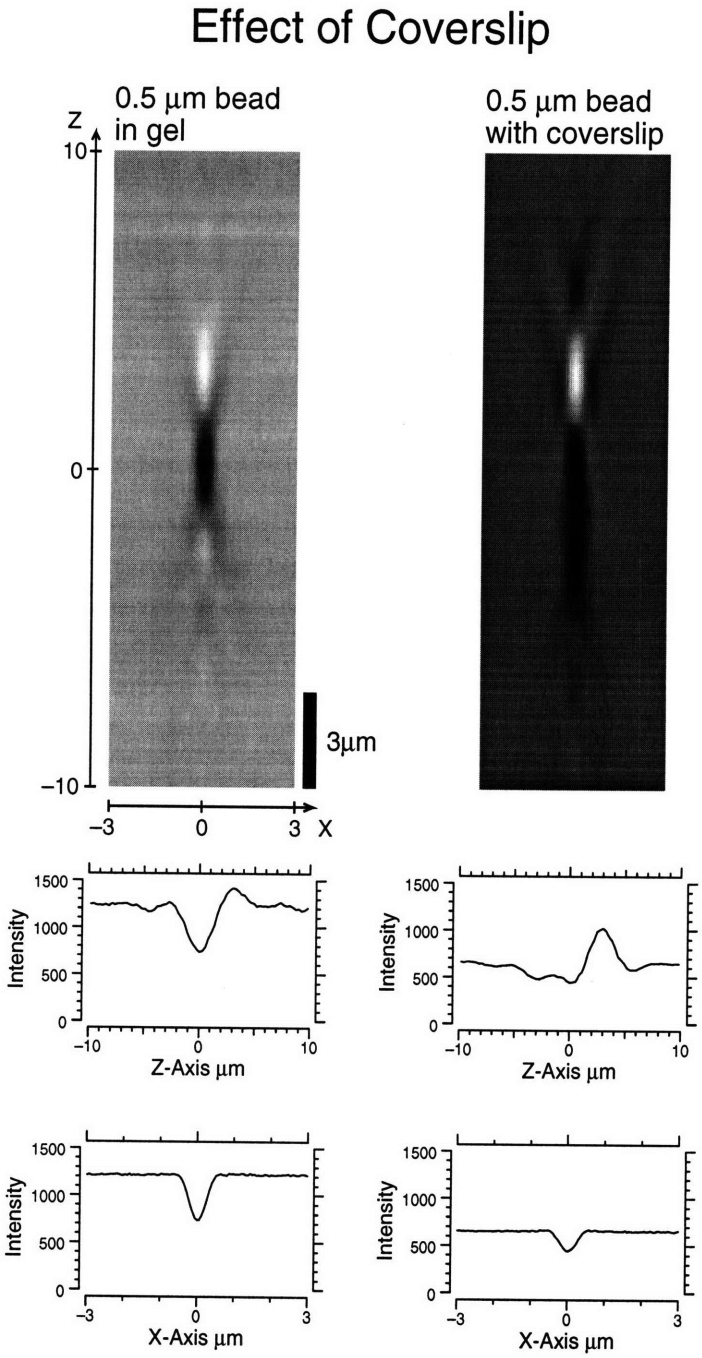

Figure 4-9: Spherical aberration in brightfield. Each image is to scale measuring 6 μm wide by 20 μm tall. The left column displays the results from a 0.5 μm microsphere mounted in gel with a 0.6 NA condenser top lens and an open condenser iris. The widths along the x and z axes are 0.52 μm and 2.5 μm respectively. The right column displays the results from a 0.5 μm diameter microsphere mounted in Mount-Quick with a coverslip and illuminated as above. The widths of the dark lobe along the x and z axes are 0.46 μm and 4.9 μm respectively.

4.5 Comparison of Results to Theory

Figure 4-10 plots four sets of data: 1) the normalized intensity of the PSF measured from a 0.2 μm microsphere in fluorescence, 2) the normalized intensity of the PSF measured from a 0.5 μm microsphere in brightfield with a condenser iris at an effective NA of 0.7, 3) the normalized intensity of the razor blade line spread function measurement (LSF), and 4) the normalized intensity of the theoretical PSF.

The waveforms are normalized by mapping the extremum to one, and mapping the average value of the background intensity to zero as described in Chapter 3. As a result, the brightfield data has been flipped about the horizontal axis so that the peak is positive with respect to the background. This facilitates the comparison of PSF measurements from different types of microscopy.

According to Equation 2.6, the PSF in focus on the xy plane should have a width of about 0.52 μm. In fluorescence, and from razor blade measurements, the data indicates a PSF width of about 0.40 μm. In brightfield, the measured data indicates a PSF width of about 0.58 μm. Equation 2.7 predicts the PSF along the optical z axis to extend about 2.45 μm. The measured data indicates 3 μm for fluorescence, 3.3 μm for brightfield, and 3.8 μm for the LSF.

Notice that the LSF along the z axis is greater in magnitude than the other measurements within 8 μm of the peak. The LSF obtained from the razor blade data was expected to be an approximation of the PSF. More precisely, the LSF is the summation of a series of overlapping PSFs arranged in a straight line. An xz slice of a LSF situated along the y axis will consist of a contribution from the PSF in the plane plus the contribution from a series of PSFs successively further from that plane. Each contribution to the LSF is identical to one of the xz slices in the PSF. The sum of all of the xz slices in the PSF will therefore yield the LSF. Figure 4-11 compares the LSF to the summation of the fluorescence measurement. The summation was acquired by adding the intensity values along every line in the y direction of the original two-point corrected volume of data.

The values of the summation of the fluorescence PSF measurement are slightly

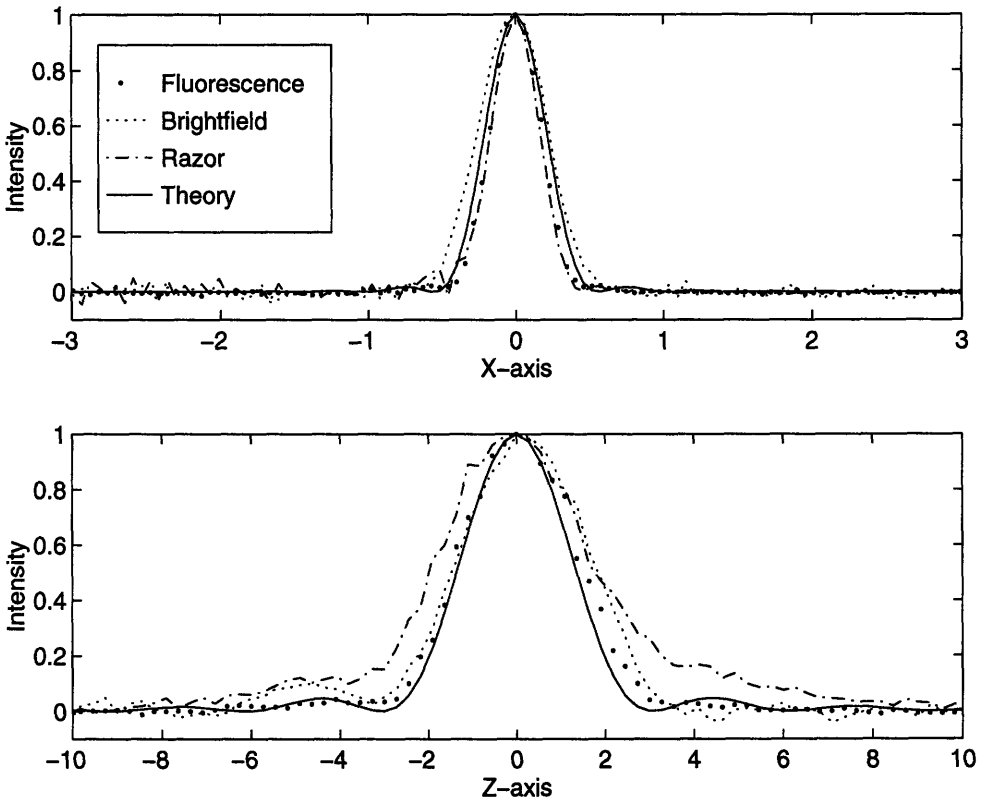

Figure 4-10: Comparison of measured data and theoretical prediction. The heavy dotted line is a measurement from a 0.2 μm microsphere in fluorescence microscopy. The light dotted line and the dash dotted line are measurements from a 0.5 μm microsphere and a razor blade respectively, both in brightfield microscopy. The solid line is the predicted PSF for an objective with aperture radius a of 2.449 mm, and focal length f of 4.11 mm. All data in this plot has been normalized by mapping the peak intensity value of each waveform to unity.

greater than the razor blade values beneath the maximum. This can partially be attributed to the fact that there was a microsphere off-center yet adjacent to the microsphere from which the fluorescence data was originally taken. Part of the PSF from the adjacent microsphere caused slightly higher intensities to be measured.

The other two sets of data in Figure 4-11 show the fluorescence measurement and its least squares best fit to the microscope model in Chapter 2. Both the x and z axes were weighted equally in the least squares fit. The best fit occured when setting the parameter for the focal distance, f to be 4.11 mm, and the finite aperture, a to be 2.423 mm. Recall the measurement of the back aperture of the objective led to an estimate of the aperture radius to be 2.449 mm.

4.6 Index of Refraction of Gel

When viewing a purely gelatin target with thickness t of about 1 mm, the difference between the specimen stage positions required to focus at the base of the gel as described in Chapter 3 is 260 microscope steps, or 23.6 μm. From Equation 3.4 the index of refraction of gel is 2.4% greater than the index of MAE. The concentration of sucrose in the MAE solution is expected to determine the index of refraction of MAE. The index of refraction of a 50 mmol/L sucrose solution is 1.3355 [11]. The index of refraction of gel is therefore 1.368. This value is within 2.6% of the index of refraction of water.

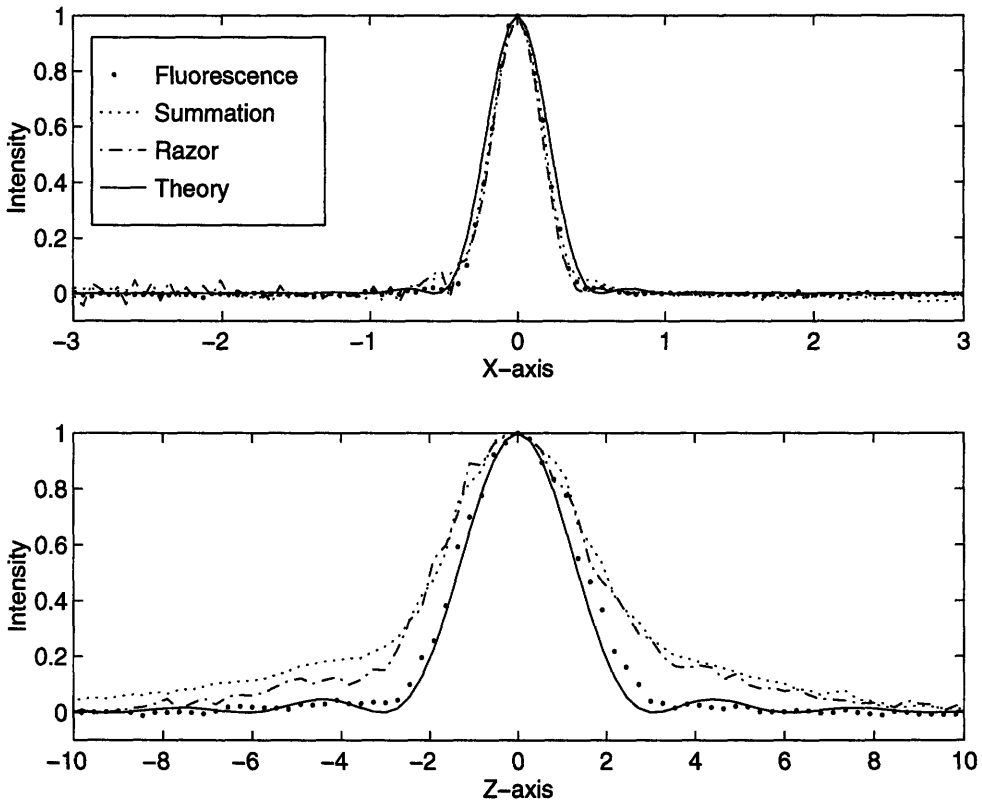

Figure 4-11: Comparison of the measurement of a razor blade (dashed dotted line) in brightfield with the summation of the measurement of the 0.2 μm microsphere (light dotted line) in fluorescence. The heavy dotted line is a measurement from a 0.2 μm microsphere in fluorescence microscopy. The solid line is the least-squares best fit to this fluorescence data.

Chapter 5

Discussion

5.1 Repeatability of Measurements

Figure 4-1 displays the repeatability of the PSF measurement. The ratio of the energy in these waveforms compared to their differences is on average, about 18 dB. This ratio is not corrected for subpixel shifts in the waveforms, and should therefore be treated as a lower bound. It is interesting to note that the correlation between measurements of the same microsphere taken on the same day iss not greater than the correlation between measurements of different microspheres taken on different days. This fact is a clear indicator that these PSF measurements are robust. Therefore, the PSF of an objective need only be measured once. There is no need to recalibrate the PSF every time the microscope is to be used.

As evidenced by its repeatability, the damped ringing observed in the PSF is not the result of noise. It is clear that the PSF is asymmetrical in z, and exhibits a much stronger checkerboard pattern beneath the microsphere than it does above the microsphere.

5.2 Fluorescence Microscopy

Of the different methods of measuring the PSF, fluorescence works best. For a 0.2 μm microsphere, the ratio of the energy between the signal and the background noise is 40

dB. For the larger 0.5 μm microsphere in brightfield, the ratio of energy between the signal and the background noise is 34 dB. With fluorescence, one can increase contrast by simply increasing the exposure time of each picture. Fluorescence also removes the effect of the condenser stage, and gives results that are closest to the model.

5.3 Brightfield Microscopy

The most striking feature of the measurements in brightfield is the existence of the bright spot. The PSF is primarily bright above the microsphere, and primarily dark below the microsphere when using a condenser stage whose effective NA is below that of the objective as shown in Figures 4-3, 4-4 and 4-5. Although this result is consistent with those reported by others [4], the existence of the bright spot is initially quite curious. At first glance, one would expect the effect of a light absorbing microsphere in the region of focus to be responsible for a reduction in the measured light intensity. One would not normally expect an increase in measured light intensity to be caused by a primarily light absorbing object.

5.3.1 Effect of Microsphere Size

Although a 0.5 μm microsphere is 150% larger in diameter than a 0.2 μm microsphere, the PSF measurements from a 0.5 μm microsphere are only 0% to 40% larger than the PSF measurements of a 0.2 μm microsphere along the x direction. As shown in Figure 4-10, the PSF in brightfield is slightly larger than in fluorescence. This fact does not reflect a fundamental difference between fluorescence and brightfield microscopy. In fact, this occurrence is merely the result of using a larger microsphere. Figure 4-3 illustrates a PSF of more comparable size from a 0.2 μm microsphere in brightfield. The extent of the measurements in the z direction were not significantly different between microspheres of either size. This indicates that a 0.2 μm microsphere does accurately approximate an impulse.

However, when evaluating the effects of a coverslip, or other aberration, the 0.2 μm microsphere often does not supply enough contrast to provide a useful image. In fact,

the 0.2 μm microsphere only provides about one third of the contrast as a 0.5 μm microsphere under the best of conditions in brightfield illumination. Attempting to image a 0.2 μm microsphere mounted in Mount-Quick underneath a coverslip is very difficult. For the evaluation of aberrations on the PSF, 0.5 μm microspheres were more effective.

5.3.2 Effect of Condenser Iris NA

The intensity value of the the apparently empty volume, or background, is highly variable across different experiments. This occurrence is primarily due to the fact that the intensity of the tungsten bulb is altered to maximize the contrast in the image between different experiments. Among the condenser iris experiments, however, the change in background intensity is only the result of the change in the setting of the condenser iris: when the condenser iris is mostly closed, there is less light to illuminate the specimen.

All measurements using the 0.6 NA top lens exhibit a bright spot in the PSF as shown in Figure 4-3. However, when using the 0.9 NA top lens, the bright spot only appears when closing the condenser iris to an effective NA less than 0.7 as shown in Figures 4-4 and 4-5. Interestingly, the contrast in the images is greatest at a condenser iris NA of 0.5. There is a strong dependence of the intensity of the bright spot on the effective NA of the condenser stage.

If the objective is used in brightfield microscopy in the usual Köhler illumination style (the condenser iris NA set at 0.7, almost completely filling the NA of the objective), then the brightfield PSF is nothing more than the fluorescence PSF in reverse video. This can be described mathematically: let F(P, NA) denote the PSF in fluorescence, and Br(P, NA) denote the PSF in brightfield. Then,

$$\mathrm{Br}(\mathrm{P},\mathrm{NA}) = \alpha(1 - \mathrm{F}(\mathrm{P},\mathrm{NA})) \tag{5.1}$$

is the correct relationship where α is a scaling constant, P is the position, and NA is the numerical aperture of the objective. However, if the objective is not illuminated

with the NA of the condenser stage completely filling the NA of the objective, then Equation 5.1 does not hold, and the basic theory does not apply.

5.4 Effect of Aberrations

5.4.1 Chromatic Aberration

A previous study [4] did not use a filter to limit the wavelengths of light used to illuminate the subject. Aberrations from a range of wavelengths focusing in different locations are called chromatic aberrations, and these effects are shown in Figure 4-7.

Chromatic aberrations do not appreciably affect the measurements in the plane of focus. However, they double the extent of the PSF in the z direction. Different wavelengths of light focus on slightly different planes and smear the PSF in the z direction. Given that the theoretical PSF scales by a factor of (a/f) (Equations 2.4, 2.5) for all axes, it is impossible to scale the theoretical PSF along the x and y axes without also scaling along the z axis. It is not possible to fit the measured data skewed by spherical aberration with a simple scaling of the theoretical model. Therefore, it is not surprising that previous studies were also unable to match measured data to theoretical predictions [4].

5.4.2 Spherical Aberration

The effect of a coverslip on the PSF measurement in brightfield illumination is to yield a measurement strikingly similar to that obtained from a microsphere in gel illuminated with an effective condenser NA of 0.3. There could be a relationship between the effective condenser NA and spherical aberration caused by the coverslip.

The condenser stage used in this study is not corrected for spherical aberrations. However, the results in Figure 4-10 indicate that if spherical aberrations from the condenser stage do exist, they are very small. Fluorescence microscopy is completely independent from the effect of the condenser stage. The measurements of the PSF in fluorescence are very similar to those taken in brightfield in Köhler illumination. If

spherical aberrations from the condenser are significant, one would expect to see a greater stretching of the brightfield PSF in the z direction. For example, Figure 4-8 illustrates the effects of spherical aberration caused by one coverslip in fluorescence microscopy. This mode of aberration is not observed in brightfield microscopy measurements taken with a gel target.

The other possible source of spherical aberration is from the gel in the target. However, the gel used is very thin, and the index of MAE and gel are both very close to that of water. Therefore, it is unlikely that any significant spherical aberrations resulted from the targets themselves.

5.5 Comparison of Results to Theory

As shown in Figures 4-10 and 4-11, the measured data fits well to the theoretical model near the region of focus. The ringing in intensity is predicted to be symmetrical both above and below the plane of focus. However, in both fluorescence and in brightfield microscopy under Köhler illumination, the ringing is mostly observed below the plane of focus. No ringing is observed within the plane of focus unless the effective NA of the condenser is about half that of the objective.

The least squares fit to the fluorescence PSF estimates the parameter for the objective aperture a to be 2.423 mm. The measurement of the back focal plane estimates the parameter for the objective aperture a to be 2.45 mm. The similarity of these two results inspires confidence in the methods used in this study.

The derivative of the step response measurement from a razor blade or an optical slit yields the LSF. The LSF is nothing more than the convolution of a series of PSFs. The PSF spreads out such that a line of closely spaced PSFs have significant and measurable overlap. Others have claimed that the LSF is equivalent to the PSF if the PSF is circularly symmetric [10]. Although the LSF is justly a rough approximation of the PSF, it is not equivalent. This technique used by Young et.al. [10] to measure the PSF, although yielding a rough approximation, is fundamentally flawed and misleading.

Figure 4-11 shows that the LSF is empirically different than the PSF. The summation of the fluorescence PSF tracks the line spread function, which supports the theory that the optics in the microscope can accurately be described as a linear system.

5.6 Bright Spot: A Possible Explanation

The basic theory does not explicitly account for the light refracted nor the light diffracted by the object in the specimen plane. If the target is primarily light absorbing, one obvious approach to explain the existence of the bright spot is to take the diffraction phenomenon into account. Imagine that in addition to a condenser iris, there existed an objective iris at the back focal plane of the objective. The only purpose of this objective iris is to control the effective NA of the objective. Consider the case where both the condenser iris and the objective iris are set at a NA of 0.4. The brightfield PSF in this case should correspond to Equation 5.1. Now imagine the objective iris is opened to an effective NA of 0.5. The extra light collected by the objective will only consist of light diffracted by the target. Assuming the target is completely light absorbing, this diffracted light will be 180 degrees out of phase with the transmitted light. If the condenser iris is also opened to a NA of 0.5, then the transmitted light at the appropriate angles will interfere with the diffracted light and form the inverted fluorescence PSF on the image plane. However, if the condenser iris remains at 0.4, there is nothing for this extra ring of light to interfere with. Therefore, an incompletely illuminated objective should have a PSF that will take a modified form of Equation 5.1

$$\mathrm{Br}(\mathrm{P}, \mathrm{NA}) = \alpha(1 - \mathrm{F}(\mathrm{P}, \mathrm{NA_c})) + \beta(\mathrm{F}(\mathrm{P}, \mathrm{NA_o}) - \mathrm{F}(\mathrm{P}, \mathrm{NA_c})) \tag{5.2}$$

where α and β are scaling factors, P is position, $\mathrm{NA_o}$ is the NA of the objective, and $\mathrm{NA_c}$ is the NA of the condenser.

5.7 Conclusion

The goals of this thesis are 1) to characterize a state-of-the-art Zeiss Axioplan microscope, 2) to compare results to theories, and 3) to describe a simple and accurate method for measuring the PSF. The system is characterized in four different ways, giving consistent results for each method. In brightfield illumination, the system is characterized by measuring a step response as well as by directly measuring an impulse response. Fluorescence microscopy is used to measure an impulse response. Finally, a clever method designed to precisely measure the radius of aperture of the objective is employed to confirm the correct parameters to use in the theoretical model. The combination of these four methods validates the measured PSF reported here.

Fluorescence microscopy is the best way to measure the PSF of a microscope objective. Fluorescent microspheres are easily accessible from vendors, and are easily visualized against a dark background. The microspheres are easy to find in fluorescence, and yield a robust measurement of the PSF.

Bibliography

[1] Born and Wolf. *Principles of Optics.* Pergamon Press, Oxford, 1965.

[2] Savile Bradbury. *An Introduction to the Optical Microscope.* Oxford University Press–Royal Microscopy Society, Oxford, 1984.

[3] C. Q. Davis, and D. M. Freeman. Using video microscopy to measure 3D cochlear motions with nanometer precision, In: Association for Research in Otolaryngology; Abstracts of the 20th Midwinter Research Meeting, St. Petersburg, FL, 1997.

[4] Kristin J. Dana. Three Dimensional Reconstruction of the Tectorial Membrane: An Image Processing Method using Nomarski Differential Interference Contrast Microscopy. Master's thesis, Massachusetts Institute of Technology, Cambridge, MA, 1992.

[5] Joseph W. Goodman. *Introduction to Fourier Optics.* McGraw Hill Book Company, New York, 1968.

[6] Sarah Frisken Gibson and Frederick Lanni. Diffraction by a circular aperture as a model for three-dimensional optical microscopy. *Journal of the Optical Society of America A.* Vol. 6, No. 9 September 1989.

[7] Halliday and Resnick. *Fundamentals of Physics Volume 2.* John Wiley & Sons, New York, 1988.

[8] Becky Hohman. 40x water immersion specifications. Carl Zeiss, Inc. Correspondence, January 8, 1997.

[9] Shinya Inoue. *Video Microscopy.* Plenum Press, New York, 1986.

[10] I.T. Young et. al. Depth-of-Focus in Microscopy, Proceedings of the 8th Scandinavian Conference on Image Analysis, Tromsoe, May 25-28, 1993.

[11] CRC Handbook of Chemistry and Physics 66^{th} Edition, CRC Press, Inc., Boca Raton, FL, 1985.